

Seismo-acoustic analysis of debris-flow events at Illgraben (Switzerland): relating signal features to flow measurements and infrasonic source mechanisms

Giacomo Belli¹, Fabian Walter², Brian W McArdell³, Duccio Gheri⁴, and Emanuele Marchetti¹

¹Department of Earth Sciences, University of Firenze

²Swiss Federal Institute for Forest, Snow and Landscape Research (WSL)

³Swiss Federal Institute for Forest, Snow and Landscape

⁴University of Florence

November 22, 2022

Abstract

We present a seismo-acoustic analysis of the debris-flow activity between 2017 and 2019 at the Illgraben catchment (Switzerland). To understand fluid dynamic processes involved in the seismo-acoustic energy generation by debris-flows, seismic and acoustic amplitudes (maximum root mean square amplitude, RMSA) and peak frequencies are compared with flow measurements (front velocity, maximum flow depth and density). Front velocity, maximum depth, peak discharge and peak mass flux show a positive correlation with both infrasonic and seismic maximum RMSA, suggesting that seismo-acoustic radiation is controlled by these flow parameters. Comparison between seismo-acoustic peak frequencies and flow parameters reveal that, unlike seismic signals, characterized by a constant peak frequency regardless of the magnitude of the flow, infrasound peak frequency decreases with increasing flow velocity, depth and discharge. Based on all collected evidence, we suggest that infrasound signals of debris-flows are generated by flow waves and water splashes that develop at the free-surface of the flow, whose dimension scales with flow magnitude. According to fluid dynamics, such surface oscillations are mostly generated wherever the flow encounters significant channel irregularities, such as topographic steps and planform steep bends, that therefore likely constitute preferential sources of infrasound. As for seismic waves, results are consistent with previous theoretical models and field observations, which attribute debris-flow seismicity to solid particle collisions, friction and fluid dynamic structures. Finally, the observed positive correlations between seismo-acoustic signal features and flow parameters highlight the potential to use infrasound and seismic measurements for debris-flow monitoring and risk management.

Hosted file

essoar.10510019.1.docx available at <https://authorea.com/users/534045/articles/598371-seismo-acoustic-analysis-of-debris-flow-events-at-illgraben-switzerland-relating-signal-features-to-flow-measurements-and-infrasonic-source-mechanisms>

Seismo-acoustic analysis of debris-flow events at Illgraben (Switzerland): relating signal features to flow measurements and infrasonic source mechanisms

Giacomo Belli¹, Fabian Walter², Brian McArdell², Duccio Gheri¹, Emanuele Marchetti¹

1. *Department of Earth Sciences, University of Firenze, via G. La Pira, 4, 50121, Firenze, Italy*
2. *Swiss Federal Institute for Forest, Snow and Landscape Research (WSL), Zürcherstrasse 111, 8903, Birmensdorf, Zurich, Switzerland*

Key points: infrasound, seismic waves, mass movements

Abstract

We present a seismo-acoustic analysis of the debris-flow activity between 2017 and 2019 at the Illgraben catchment (Switzerland). To understand fluid dynamic processes involved in the seismo-acoustic energy generation by debris-flows, seismic and acoustic amplitudes (maximum root mean square amplitude, RMSA) and peak frequencies are compared with flow measurements (front velocity, maximum flow depth and density). Front velocity, maximum depth, peak discharge and peak mass flux show a positive correlation with both infrasonic and seismic maximum RMSA, suggesting that seismo-acoustic radiation is controlled by these flow parameters. Comparison between seismo-acoustic peak frequencies and flow parameters reveal that, unlike seismic signals, characterized by a constant peak frequency regardless of the magnitude of the flow, infrasonic peak frequency decreases with increasing flow velocity, depth and discharge. Based on all collected evidence, we suggest that infrasonic signals of debris-flows are generated by flow waves and water splashes that develop at the free-surface of the flow, whose dimension scales with flow magnitude. According to fluid dynamics, such surface oscillations are mostly generated wherever the flow encounters significant channel irregularities, such as topographic steps and planform steep bends, that therefore likely constitute preferential sources of infrasound. As for seismic waves, results are consistent with previous theoretical models and field observations, which attribute debris-flow seismicity to solid particle collisions, friction and fluid dynamic structures. Finally, the observed positive correlations between seismo-acoustic signal features and flow parameters highlight the potential to use infrasound and seismic measurements for debris-flow monitoring and risk management.

Plain language summary

Debris-flows represent a serious hazard in mountain environments and significant efforts are undertaken to develop automatic warning systems. We present a seismo-acoustic analysis of the debris-flows at the Illgraben (Switzerland) between 2017-2019. A positive correlation emerges between flow parameters and the amplitude of generated infrasonic (low-frequency sound) and seismic (ground vibrations) signals, suggesting that the seismo-acoustic radiation by debris-flows

scales linearly with flow discharge. Moreover, while seismic signals are characterized by a constant peak frequency regardless of the magnitude of the flow, infrasound peak frequency decreases with increasing front velocity, depth and discharge. These results, in agreement with previous models and observations, suggest a decoupled source mechanism of the infrasound and seismic signals. For the seismic signal, presented results agree with previous models, which attribute the radiation of seismic waves to solid particle collisions, friction and fluid dynamic structures. Our novel observations allow to improve our understanding of the infrasound source, being consistent with turbulence-induced waves at the flow free-surface, explaining the signal with respect to flow properties and channel irregularities. Moreover, experimental results highlight how infrasound and seismic measurements could be successfully used to quantify remotely the magnitude of debris-flows, thus opening new perspective for monitoring and risk management.

1. Introduction: Debris-Flows

Debris-flows are episodic gravitational currents of high density ($\sim 2000 \text{ kg/m}^3$ (Wang et al., 2018)), consisting of highly concentrated mixtures of water, mud and solid debris particles in varying proportions (Coussot and Meunier, 1996). Their flow behavior has been described as intermediate between floods and landslides (e.g. Iverson and Vallance, 2001). Within debris-flows, the solid fraction typically ranges between 50 and 90 % (Coussot and Meunier, 1996), with solid particle sizes varying from clay to meter-sized boulders (Perez, 2001).

Occurring on steep slopes of loose debris, debris-flows are often initiated by water supply (Badoux et al., 2009), typically via intense rainfalls, natural or artificial dams collapses or rapid snowmelt (Takahashi, 1981; Liliboutry et al., 1977; Dowling and Santi, 2014). Debris-flows tend to occur as several surges (Iverson, 1997) that flow long distances in steep torrential channels, with volumes commonly exceeding thousands of m^3 (Coussot and Meunier, 1996; Iverson, 1997). Typical debris-flow velocities range between 0.5 and 10 m/s (Sharp and Nobles, 1953; Johnson, 1970; Pierson, 1980), although velocities up to 20 m/s have been reported (Khegai et al., 1992).

Based on flow dynamics and solid fraction, a debris-flow can be subdivided in three main flow parts: the boulder-rich front, the flow body and the flow tail (Coussot and Meunier, 1996; Costa and Williams, 1984; Iverson, 1997). The boulder-rich front transports rocks of all sizes and mud and acts as a granular flow with high solid fraction (50-90%) (Iverson, 1997). It resists the overall gravity-driven motion as the flow body pushes it from behind (Johnson and Rodine, 1984; Iverson, 1997). The flow body is a debris-laden flow with high solid fraction (50-90%) but richer in mud than in boulders and thus it behaves more fluid and with lower basal friction than the front. The flow tail typically consists of a two-phase hyperconcentrated flow, with a lower solid fraction (40-55%) (Pierson, 1985) and is characterized by a significant relative velocity between water-solid suspension and coarser solid particles (Smart and Jäggi, 1983; Coussot and Meunier, 1995), which, due to a reduced flow transport capacity, begin

to settle (Cousot and Piau, 1994).

The destructive potential of debris-flows, resulting from their high impact forces and their long runout distances, combined with their relative unpredictability, renders debris-flows among the most dangerous natural hazards in mountain environments (Badoux et al., 2009). In addition, due to climate change and to an increased population pressure in mountain areas, the impact of debris-flows on human lives and activities has increased in the last decades (Dowling and Santi, 2014). Nevertheless, the moderate flow velocities (typically < 10 m/s) make early warning possible if debris flows are detected rapidly upon their formation (Arattano and Marchi, 2005; Badoux et al., 2009).

Due to the complexity of the phenomenon and to the wide variability of flow types, geomorphologic features of the catchment and socio-economic settings of the affected areas, debris-flow monitoring is based on a wide range of approaches (see Arattano and Marchi, 2005 and Hurlimann et al., 2019, for a review), involving rainfall forecast, catchment observations and in-channel measurements (Badoux et al., 2009). Recently, the use of seismic and infrasonic signals for the study and monitoring of debris-flows has received scientific attention (Arattano, 1999; Burtin et al., 2009; Burtin et al., 2014; Walter et al., 2017; Lai et al., 2018; Marchetti et al., 2019). As a matter of fact, debris-flows radiate elastic energy both into the ground and into the atmosphere, in the form of seismic waves and infrasound, respectively (Marchetti et al., 2019). These signals typically have emergent, cigar-shaped envelopes (Lai et al., 2018; Marchetti et al., 2019) and show a wide variability in duration and amplitude.

Similar to what is observed for seismic energy radiation by rivers (Burtin et al., 2008; Tsai et al., 2012; Gimbert et al., 2014), both theoretical and experimental studies suggest that within a debris-flow seismic waves are generated by solid particle-bed collisions driven by friction, bed load transport and fluid dynamic effects (Schmandt et al., 2013; Kean et al., 2015; Lai et al., 2018). These processes produce fluctuations of the basal force exerted by the flow on the bed radiating high frequency seismic waves. In particular, particle collisions with the bed occur both in the form of single particle random impacts and in the form of force chains, which are networks of interacting particles that amplify the collision forces to the bed (Estep and Dufek, 2012; Zhang et al., 2021(b)). Although seismic energy is radiated along the entire debris-flow, the boulder-rich debris-flow front appears to dominate seismic signal generation (Farin et al., 2019; Zhang et al., 2021(a)). This was confirmed also by Coviello et al., (2019), who analyzed the seismic energy produced by debris flows in the Gatria stream catchment (Eastern Italian Alps) showing that most energy transfer occurs during the passage of the surge fronts and is controlled by the mass and the velocity of each surge. Peak frequencies of debris-flow seismic signals appear to depend only on source-to-receiver distance (Tsai et al., 2012; Burtin et al., 2009; Lai et al., 2018; Wenner et al., 2019), with peak frequencies decreasing with increasing distances from the flow front, due to stronger attenuation of higher seismic frequencies.

Propagating as elastic air waves, infrasound is generated whenever the atmosphere is perturbed by a rapid movement. Marchetti et al. (2019) performed an array analysis of infrasound signals generated by three debris-flows at the Illgraben (Switzerland). They modeled the generated infrasound as an incoherent superposition of signals resulting from multiple, simultaneously active acoustic sources along the flow. However, in agreement with experimental observations on rivers, infrasound radiation of debris-flows is also affected by fixed locations along the channel, whenever the flow travels across dams or topography changes (Kudo, 1993; Feng et al., 2014, Marchetti et al., 2019; Belli et al., 2021). Specifically, in steep mountain channels infrasound is likely produced at dams as shooting water hits the stream bed downstream and triggers surface waves and splashes induced by turbulence that develops at the base of the free overfall (Tokyay and Yildiz, 2007). Feng et al. (2014), according with previous models based on large objects impacting water (Ostrovsky and Bedard, 2002), modeled infrasound waves generated at dams as the result of surface waves induced by water entering an absorption pool. In particular, they suggest a mechanism where water fall at dams generates local elevations of the water surface surrounded by rings of descending water levels which radiate infrasound as a dipole source (Feng et al., 2014). Therefore, debris-flows, similar to rivers, are expected to have multiple sources of infrasound, according with flow dynamics and channel geometry (Marchetti et al., 2019). Unlike rivers, peak frequency of infrasound signals produced by debris-flows is typically concentrated below 40 Hz (Chou et al., 2013) and seems to scale with flow volumes (Marchetti et al., 2019).

Seismo-acoustic networks have proven to be powerful tools for the study of mass movements, such as pyroclastic density currents and snow avalanches (Yamasato, 1997; Allstadt et al., 2018; Ulivieri et al., 2011; Vilajosana et al., 2008; Ripepe et al., 2009), providing crucial information also on debris-flows, such as estimates of volume, discharge, velocity and timing of events (Lai et al., 2018; Marchetti et al., 2019; Schimmel et al., 2021). Concerning debris-flows, most efforts focused on the early detection of the events (Arattano, 1999; Walter et al., 2017; Lai et al., 2018; Chmiel et al., 2021). However, the radiation processes of both infrasonic and seismic wavefields during debris flow activity are still unclear, due to the complexity and the variability of the generating mechanisms and their chaotic superposition that results in emergent and sustained signals which lack impulsive and distinct phases (Wenner et al., 2019; Coviello et al., 2019; Marchetti et al., 2019). As a result, it is not yet fully understood how flow behavior and processes affect and control resulting seismo-acoustic signal features and, to our knowledge, an accurate infrasound source model for debris-flows is still missing.

In this study, we present a seismo-acoustic analysis of debris-flow activity in the Illgraben catchment (Switzerland) during summers 2017-2019. The main features, such as maximum amplitude and peak frequency, of infrasonic and seismic signals are compared with flow measurements in order to investigate what fluid dynamic or physical processes control the seismo-acoustic energy

radiation within debris-flows.

1. Study Site and Monitoring System

The Illgraben catchment, situated in Switzerland's Canton Valais, (Figure 1), is one of the most active debris-flow basins in the Alps (Badoux et al., 2009) and among the best instrumented sites worldwide. The catchment has an area of $\sim 10 \text{ km}^2$ (Schlunegger et al., 2009) and an elevation that ranges from the 2716 m (Above Mean Sea Level) of the Illhorn mount to the 850 m (AMSL) of the debris fan apex (Badoux et al., 2009). The upper basin ($\sim 5 \text{ km}^2$) is drained by the steep Illgraben torrent that, after a $\sim 5 \text{ km}$ path ($\sim 3 \text{ km}$ in the active upper catchment, until the fan apex and $\sim 2 \text{ km}$ along the fan axis) flows into the Rhone River at an elevation of 610 m (AMSL). The Illgraben channel has an average slope of 9° (16%) in the upper basin, that decreases to 5.7° (10%) downstream of the fan apex (Badoux et al., 2009). The erosion of the stream along the upper Illgraben catchment frequently produces rockfalls and landslides along the steep ($> 40^\circ$) catchment slopes (Schlunegger et al., 2009) and provides sediment supply for Illgraben's debris-flow events (Berger et al., 2011; Bennet et al., 2013). The debris-flow activity has led, in the last 16-17 ky (Ivy-Ochs et al., 2008; Schurch et al., 2016), to the formation of the large ~ 500 million of m^3 debris fan, on the southern side of the Rhone valley (Schlunegger et al., 2009; Badoux et al., 2009), which nowadays is densely inhabited.

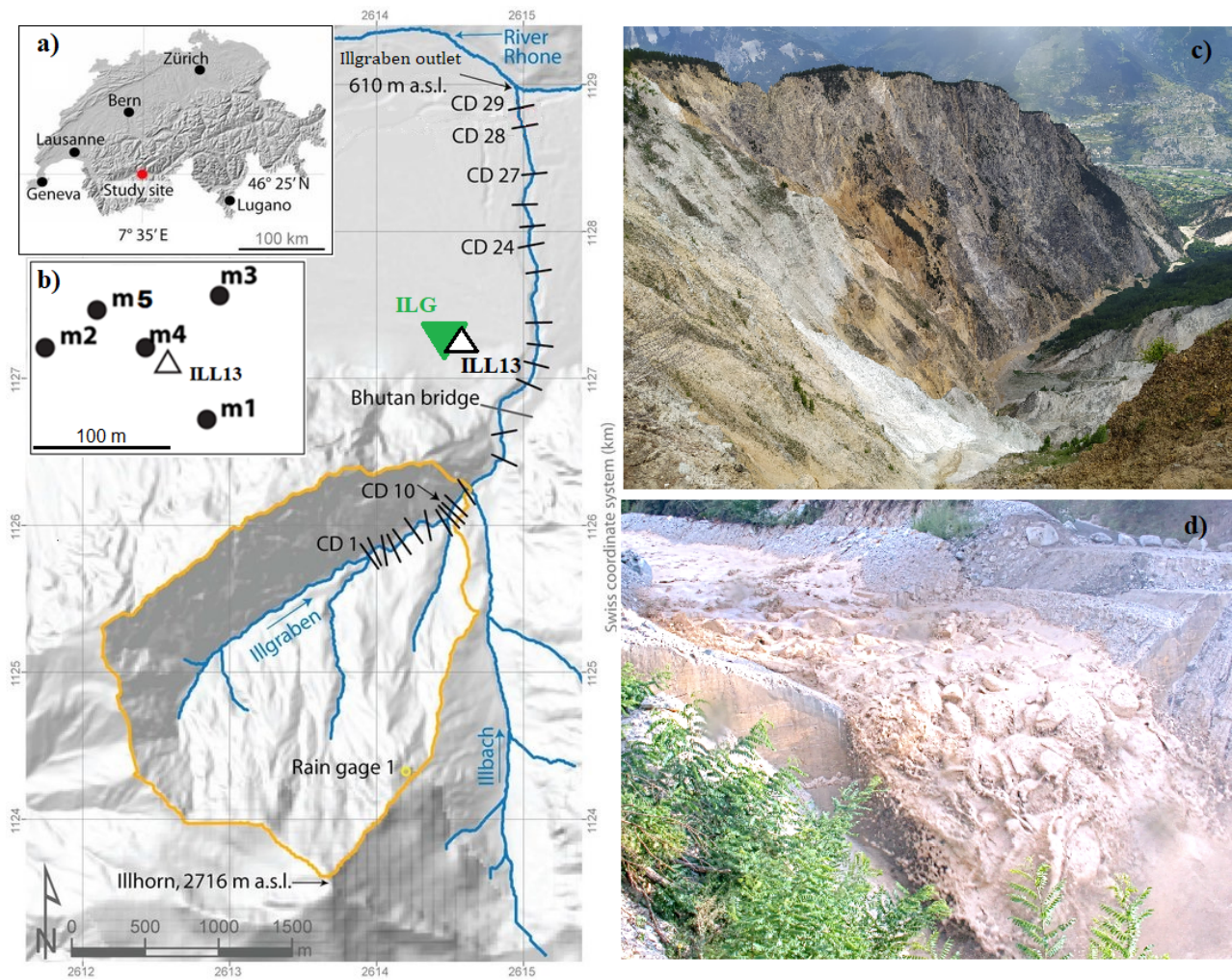


Figure 1: Left: Map of the geographic setting of the Illgraben catchment, showing the extension of the upper catchment (yellow line), the position of ILG infrasound array (green triangle) and of the ILL013 seismometer (white triangle) used in this study. The black bars with alpha-numerical labels indicate the position of Illgraben check dams (CD). (a) Position of the Illgraben in Switzerland. (b) Relative geometry of the ILG infrasound array and seismic sensor. (c) Picture of the Illgraben catchment taken from its south-west rim (source: Giacomo Belli); (d) photograph of an Illgraben debris-flow shooting over CD29 (event on 2019/08/11; source: WSL).

Debris-flows occurring in the Illgraben catchment are characterized by a considerable variability in size, duration and in the hydraulic, physical and compositional features (Badoux et al., 2009). Typical events are granular debris-flows

with high solid fraction (50-90%) and transporting blocks up to several meters in diameter, mostly concentrated in the flow front (Badoux et al., 2009; Coussot and Meunier, 1996). Other flow types occur as well, ranging from muddy debris-flows over hyperconcentrated flows to flood flows, and despite having a lower solid fraction, they may all transport boulders with a mean diameter as large as the flow depth (Badoux et al., 2009). Moreover, many of the flows occur as flash floods (Badoux et al., 2009), with the flow depth rising from zero to several meters in a short time span (few seconds or minutes), with strong implications for flow impact and associated hazard.

Typical Illgraben debris-flows have volumes of $\sim 20.000 \text{ m}^3$, but major events with volumes up to $70.000\text{-}100.000 \text{ m}^3$ are often observed (Badoux et al., 2009). While events with volumes $< 75.000 \text{ m}^3$ remain entirely within the stream channel, larger volume events may overflow the channel banks and reach inhabited areas, constituting a serious threat to local communities (Badoux et al., 2009). A wide variability, likely reflecting the solid fraction and water content variation, is also observed in flow velocity, typically ranging between 3 and 8 m/s (Wenner et al., 2019).

At Illgraben, debris-flows generally occur between May and October (Badoux et al., 2009; Berger et al., 2011). Such a clear seasonal activity results from common triggering processes, like the summer rain storms (Hürlimann et al., 2003; McArdell et al., 2007), or snowmelt (Badoux et al., 2009; Wenner et al., 2019). Debris-flow triggering is also possible in the absence of precipitation, for rapid snow melt or when natural lake dams formed by landslides sudden fail, giving rise to a critical runoff (Costa and Schuster, 1988; Evans and Clague, 1994). In particular, based on historical event analysis, the largest Illgraben debris-flow occurred in association with sudden catastrophic failure of a natural landslide-formed dam in the upper catchment (Badoux et al., 2009).

In order to mitigate the impact and risk associated with Illgraben debris-flow activity and to minimize erosion on the torrent channel (Henderson, 1996; Tokyay and Yildiz, 2007), a series of check dams (CDs) were constructed along the channel (Figure 1). This led to a significant reduction of the debris-flows damage potential; indeed, most debris flows no longer overtop the channel bank and significant damage last occurred in 1961 when a road bridge was destroyed (Badoux et al., 2009).

Since 2000, the Swiss Federal Institute for Forest, Snow and Landscape Research (WSL) installed a scientific observatory devoted to debris-flow monitoring (Rickemann et al., 2001; Hürlimann et al., 2003; McArdell et al., 2007), consisting of flow stage sensors (laser, radar (Arattano and Marchi, 2005)), geophones installed on check dams for front-velocity estimation and video cameras (Hürlimann et al., 2003), as well as a large force plate which has been used to determine bulk flow properties such as the mass density and force-fluctuations (McArdell et al., 2007; Schlunegger et al., 2009). The separate debris-flow alert system, which is under the responsibility of the local municipality, combines catchment status observations, related to general sediment availability and the possible

presence of torrent-blocking landslides, and direct in-channel flow threshold detection measurements. This system has recently been modified, but for the data presented herein it consisted of radar flow-depth measurements and geophone sensors for determining flow velocity (Badoux et al., 2009) and the force plate for density. In both the WSL scientific observatory and the operational warning system, debris-flow front arrival times are detected with geophones installed on the concrete of CDs 1, 27, and 29 (Figure 1) (Walter et al., 2017), and differences in arrival times are used to calculate the flow velocity. Recently, debris-flow activity at Illgraben has also been monitored by a dense seismic network (e.g. Walter et al., 2017; Wenner et al., 2020; Chmiel et al., 2021) and by a small aperture infrasound array (Marchetti et al., 2019).

1. Instrumental Set-Up

For this study we used infrasound and seismic data recorded on the fan apex, at a distance of ~600 m from the fan apex, and hydraulic data collected by in-torrent measurements. Infrasound data are recorded by array ILG (Figure 1), that has been installed during the debris-flow season (late spring and summer) since 2017 (Marchetti et al., 2019). ILG is a FIBRA array (www.item-geophysics.it), designed to operate with fiber optic connection of up to 5 array elements. Here, sensors are arranged in a triangular geometry (Figure 1) and an aperture (maximum distance between two array elements) of 160 m, optimized to analyze infrasound signals in the 1-10 Hz frequency band. Each array element is equipped with a differential pressure transducer with a sensitivity of 400 mV/Pa in the pressure range of ± 12.5 Pa and the frequency response ranges between 0.01 and 200 Hz. Analogue pressure data are sampled at each array element at 50 Hz and digitized at 16 bits. The installation site is a flat forested area to minimize wind noise.

Seismic data have been collected by a Lennarzt LE3D 1s triaxial seismometer with a flat response between the sensor’s natural frequency of 1 Hz and an upper corner of 100 Hz. In this work we used data from a seismic station that is collocated with the infrasonic array (ILL13, Figure 1), that is part of the dense seismic network deployed during the debris-flow season since 2016 (Wenner et al., 2020). The seismometer, deployed near the central element of the infrasonic array, is placed into a 30 cm deep pit, subsequently back-filled with soil. Ground motion is recorded with a Nanometrics Centaur digitizer. Data are collected at 100 Hz and continuously telemetered to the Swiss Seismological Service.

Debris-flow hydraulic and physical data are collected by in-torrent measurements, provided by sensors closely located along the stream path or directly within the channel, as described above. In particular we used flow-depth measurements at CD29, flow velocities calculated from arrival times at CD27 or CD28 and CD29, and flow density values estimated from force plate measurements that are performed at CD29 (Figure 1).

1. Data

4.1 The Event Database

In the period 2017-2019, 18 debris-flow were observed at Illgraben (Table 1). Events are characterized by a high variability in size, magnitude, duration and in the hydraulic features (Table 1, Figure 2). For the events in 2017 and 2018, the force plate was not operational as a result to damage during a major flow event in 2016 and the flow depth measurements and related volume calculations are less accurate than after the re-installation of the force plate in 2019. Total volumes are estimated by integrating flow discharge over the entire debris-flow wave (Schlunegger et al., 2009); obtained values vary between few thousands of m^3 and 10^5 m^3 and reveal that the majority of Illgraben debris-flows are small ($V < 20,000 \text{ m}^3$), although several large flows ($V > 80,000 \text{ m}^3$) are commonly observed (Figure 2a).

Estimated flow front velocity (v), calculated as the differences between the flow front arrival time at CD27 (or CD28) and CD29, range from $< 1 \text{ m/s}$ to $> 7 \text{ m/s}$, suggesting a wide variability in flow dynamics, probably reflecting differences in composition and water content. Typical events have front velocities between 6.5 and 7.5 m/s (50% of the events with measured velocity), while events with low velocity ($v < 2 \text{ m/s}$) are observed too (Figure 2b).

Maximum flow depth (H), ranging from $\sim 0.6 \text{ m}$ to 2.8 m , is measured at CD 29 (Walter et al., 2017; Wenner et al., 2019). Out of the 12 debris flows for which a flow depth measurement is available, a hydrometric height $\geq 2 \text{ m}$ was recorded only for 3 events (Figure 2c). Comparison between front velocity and maximum flow depth revealed that the flow velocity appears to be at least partially controlled by the flow depth, with higher flow velocity generally corresponding to larger flow depth (Figure 2d), in agreement with theory of open channel flows predicting higher velocity for larger-depth flows (Henderson, 1996). The red line in Figure 2d represents the critical velocity $v_c = \sqrt{gH}$ and therefore marks the distinction between subcritical ($v < v_c$) and supercritical flows ($v > v_c$) (Henderson, 1996). Criticality is the state at which the specific energy of the flow is minimum (Henderson, 1996), and is equal to the velocity (v_w) with which a wave or perturbation resulting from any disturbance or obstacles in open channel flow tends to propagate over the water surface (Henderson, 1996). The comparison between debris-flow front velocity and critical velocity reveals that almost all Illgraben debris-flows are supercritical flows, with only three events with $H < 1 \text{ m}$ falling into the subcritical domain (Figure 2d). In particular, we observe that all large debris-flows with $H > 1 \text{ m}$ are supercritical. This trend is reflected by the distribution observed for the Froude number (Fr) among the debris-flow events (Figure 2e), computed with the following equation valid for rectangular channels (Henderson, 1996), which is a good assumption for the Illgraben:

$$Fr = \frac{v}{\sqrt{Hg}}, \text{ (Eq. 1)}$$

where g is the acceleration of gravity. The Froude number expresses the ratio between flow velocity and the velocity ($v_w = v_c$) of any perturbation generated in the flow as the result of encountered channel irregularities and obstacles (Henderson, 1996). Computed values, listed in Table 1, confirm that Illgraben's larger

debris-flows fall into supercritical flow conditions, i.e. Froude number $Fr > 1$ (Figure 2e), indicating that the flow is faster than propagation of surface perturbations, that, therefore, are able to propagate only downstream (Henderson, 1996).

Flow bulk density (ρ) is computed as the mass/volume ratio at the force plate deployed on the brink of CD29, measuring the flow weight and the depth of the flow over the force plate and considering the plate area and channel geometry (McArdell et al., 2007; McArdell et al., 2016). Obtained values, available for 8 events, vary between 1600 and 2400 kg/m³ (Table 1), reflecting differences in solid fraction and water content.

Again, assuming a rectangular channel section, reasonable for the Illgraben, we combine front velocity, maximum flow depth and flow density values to derive the peak flow discharge per unit channel width (Q_u) and the peak mass flux per unit channel width (MF_u) as:

$$Q_u = H \bullet v , \text{ (Eq. 2)}$$

$$MF_u = Q_u \bullet \rho , \text{ (Eq. 3)}$$

Obtained values are listed in Table 1. If we assume that the width of the Illgraben channel between CD28 and CD29, where velocity and depth measurements are collected, remains constant over time, we can reasonably assume that the computed peak discharge and peak mass flux per unit channel width reflect the peak volumetric discharge and mass flux, respectively. The stable width channel assumption is reasonable considering that the Illgraben channel is stabilized by the constructions of the check dams.

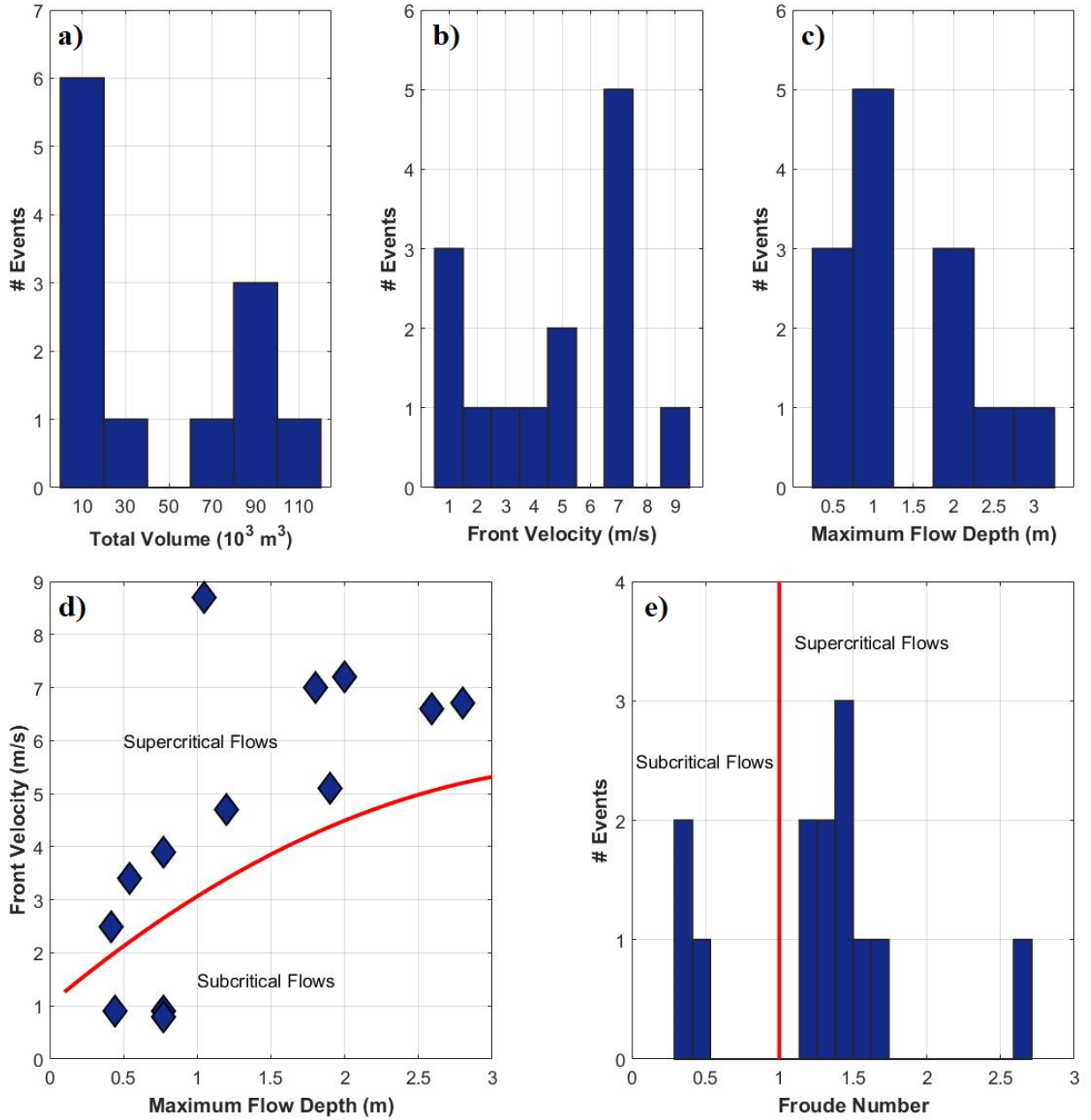


Figure 2: histograms showing the distribution of total volume (a), front velocity (b), maximum flow depth (c) and Froude number (d) among the 2017-2019

Illgraben debris-flow events. In d) the vertical red line marks the boundary between subcritical flows ($Fr < 1$) and supercritical flows ($Fr > 1$).

Table 1: Timing and hydraulic and physical features of the Illgraben 2017-2019 debris-flows. The force plate was not present in 2017-2018, consequently some parameters are reported as n.m. (not measured) and some derived quantities as n.c. (not computed). Froude number, unit peak flow discharge and unit peak mass flux are computed using Eq. 1, Eq. 2 and Eq. 3 respectively.

Date	CD1 Ar- rival Time (UT)	Volume (m ³)	Front Veloc- ity (m/s) (CD28- 29)	Maximum Flow Depth (m) (CD29)	Bulk Den- sity (Kg/m ³)	Froude Num- ber	Unit peak flow dis- charge (m ² /s)	Unit peak mass flux (t/m s)
/05/29	:58:31				n.m.			n.c.
/06/03	:27:38				n.m.			n.c.
/06/14	:30:48				n.m.			n.c.
/06/11	:46:39	n.m.	n.m.	n.m.	n.m.	n.c.	n.c.	n.c.
/06/12	:29:16	n.m.	n. m.	n.m.	n.m.	n.c.	n.c.	n.c.
/07/25	:56:40	n.m.			n.m.			n.c.
/08/08	:49:25	n.m.		n.m.	n.m.	n.c.	n.c.	n.c.
/06/10	:02:51							
/06/10	:01:17							
/06/20	:12:17	n.m.	n.m.	n.m.	n.m.	n.c.	n.c.	n.c.
/06/21	:34:42							
/07/01	:00:29	n.m.	n.m.	n.m.	n.m.	n.c.	n.c.	n.c.
/07/02	:09:28							
/07/03	:43:15							
/07/15	:40:21							
/07/26	:33:12							
/08/11	:02:34							
/08/20	:40:59							

4.2 The Geophysical Database

Our geophysical dataset consists of seismic and infrasonic data of the 18 debris-flow events (Figure 3a), recorded by the ILG infrasonic array and the ILL13 seismometer (Figure 1). Infrasonic data for the 2018/08/08 event are missing. Events are recorded as long lasting (30-100 min), emergent, cigar shaped infrasonic and seismic signals. Peak-to-peak seismic amplitudes span 2 orders of magnitude, ranging from ~3 m/s, observed for the 2018/06/11 and 2018/06/12 events, up to ~200 m/s, observed for the 2017/05/29 seismogram. In the infrasonic record, peak-to-peak amplitudes vary from a maximum of ~1.5 Pa, observed for the 2017/05/29 debris-flow (2 orders of magnitude above the back-

ground noise of around 0.05 Pa) down to 0.2 Pa observed for the 2019/07/15 event. The six smallest events did not produce discernible signal above noise levels (Figure 3a). The high-amplitude infrasound transients observed for several events, and clearly visible in Figure 3a, are infrasonic signals generated by lightning activity and thus not related to debris-flows (Marchetti et al., 2019). For the 2019/07/02 and 2019/07/26 debris-flows, infrasound signal produced by the rainstorm, having comparable amplitudes as the debris-flow signal, strongly affects the entire waveform (Figure 3a).

In general, seismic signals appear to be clearer, i.e. characterized by a higher signal-to-noise ratio, compared to infrasonic ones. Indeed, whereas every reported debris-flow event generated a distinguishable seismic signal, at least 6 debris-flows did not generate a distinguishable infrasound signal above the back-ground noise level (Figure 3a). Therefore, the present analysis of Illgraben debris-flows has been limited to 11 out of 18 events in case of infrasound, while it has been carried out on all 18 events in case of seismic signals (Table 2).

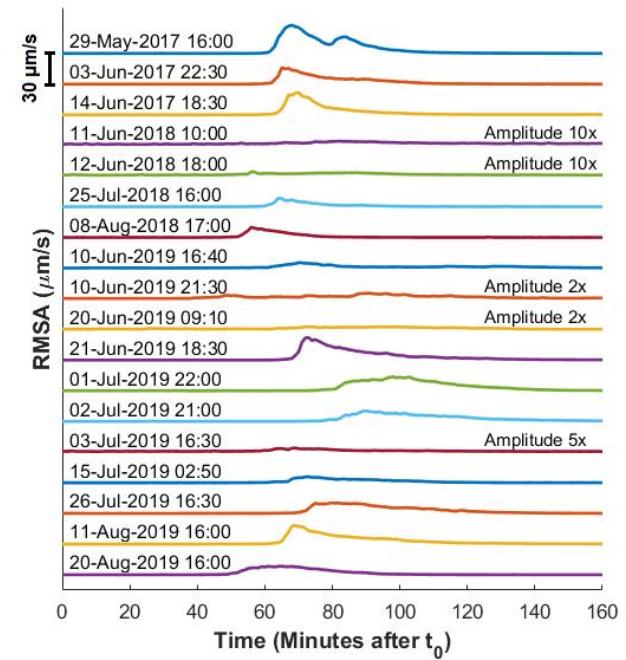
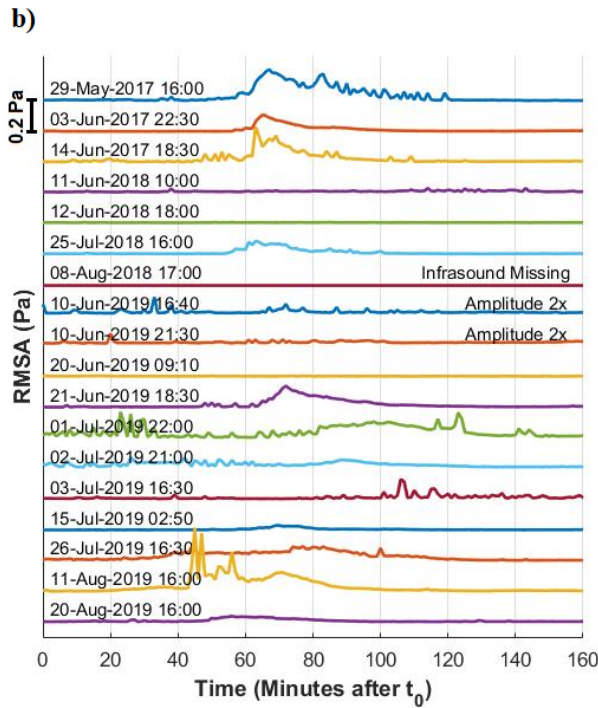
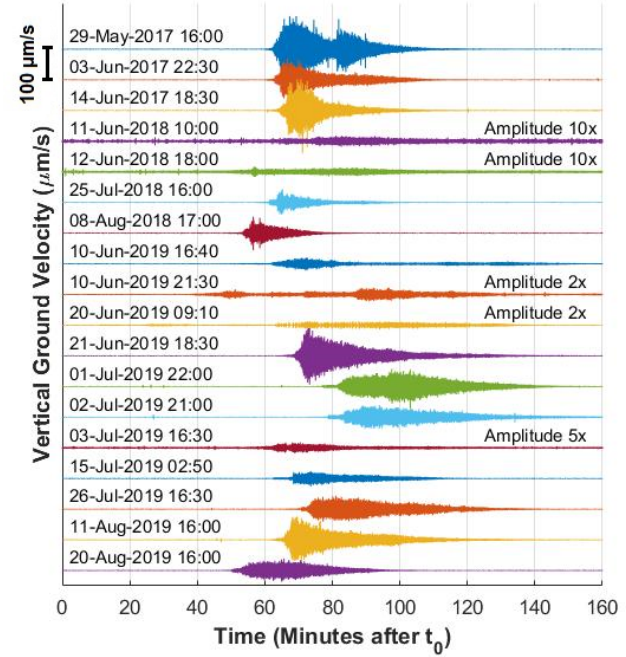
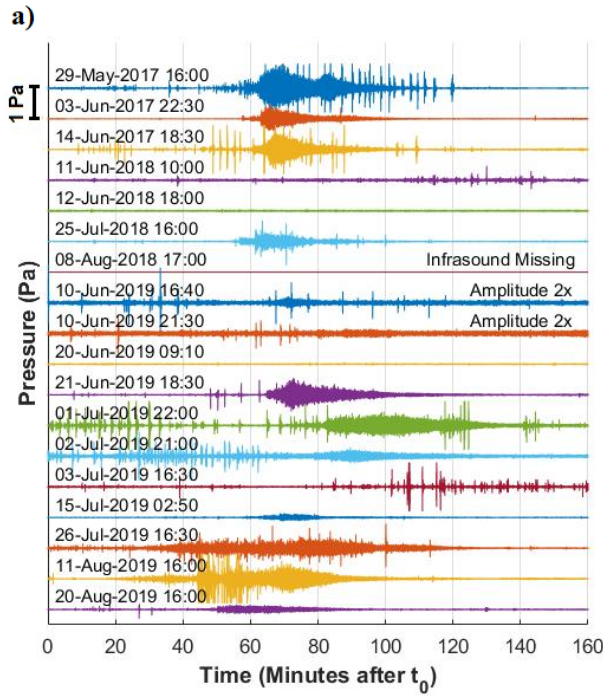


Figure 3: a) infrasound (left) and seismic (right) waveforms of the 18 debris-flow at Illgraben between 2017 and 2019. b) Infrasound (left) and seismic (right) Root Mean Square Amplitude (RMSA) envelopes computed over one-minute-long moving time windows for all 18 events. For all signals, timing is expressed in minutes after the time reported on the left of each trace.

The root mean square amplitude (RMSA) was calculated on 1-20 Hz band-pass filtered infrasound and seismic signals, over 1-minute-long moving time windows along the entire duration of the events (Figure 3b). The signal envelope, obtained from the RMSA analysis, shows a marked asymmetry resulting from an amplitude rising time that is generally shorter than the amplitude fall-off tail. The signal duration (Table 2), ranging between 96 and 163 minutes for seismic and between 68 and 145 minutes for infrasound signals, is estimated visually as the time interval when RMSA values exceed pre- and post-event background RMSA levels. Maximum RMSA varies between 0.035 and 0.208 Pa for infrasound and between 0.43 and 27.8 m/s for seismic signals (Table 2). The small variance of maximum infrasound RMSA, compared to the seismic RMSA, results from the infrasonic analysis having been performed only on the 11 events for which a clear infrasound signal was recorded; the 6 lower magnitude debris-flow events were excluded.

Table 2: Peak time, duration, maximum RMSA and peak frequency of infrasound and seismic signals. The symbol (*) marks the events for which infrasound peak frequency is strongly affected by rainstorms that occurred during the peak phase of the flow and produced infrasonic noise approximately of the same magnitude as the debris-flow signal.

Debris Flow Events	Infrasound RMSA Peak Time (UT)	Infrasound Signal Duration (min)	Max Infrasound RMSA (Pa)	Infrasound Peak Frequency (Hz)
/05/29	:07			
/06/03	:35			
/06/14	:39			
/07/25	:03			Not computable
/06/21	:42			
/07/01	:38			
/07/02	:29			Not used(*)
/07/15	:59			
/07/26	:47			Not used(*)
/08/11	:11			
/08/20	:56			

Debris Flow Events	Infrasound RMSA Peak Time (UT)	Infrasound Signal Duration (min)	Max Infrasound RMSA (Pa)	Infrasound Peak Frequency (Hz)
Debris Flow Events	Seismic RMSA Peak Time (UT)	Seismic Signal Duration (min)	Max Seismic RMSA (m/s)	Seismic Peak Frequency (Hz)
/05/29	:08			
/06/03	:35			
/06/14	:40			
/06/11	:22			Not discernible
/06/12	:56			Not discernible
/07/25	:04			
/08/08	:56			
/06/10	:50			
/06/10	:01			
/06/20	:37	Not discernible		
/06/21	:43			
/07/01	:38			
/07/02	:30			
/07/03	:39			Not discernible
/07/15	:03			
/07/26	:50			
/08/11	:09			
/08/20	:05			

Seismic and infrasound waveforms were also analyzed in the frequency domain by computing the Power Spectral Density (PSD) (Table 2). The seismic signals of the events of 2018/06/11, 2018/06/12 and 2019/07/03 are characterized by a very low signal to noise ratio, therefore the PSD was not computed for these three events. Due to the recording sensor malfunction, for the event of 2018/07/25 the infrasonic PSD is not computable. Therefore the infrasound generated by this event was excluded from the frequency analysis below. Seismo-acoustic PSD curves are shown in Figure 4. Infrasound and seismic signals are marked by significantly different peak frequencies. Infrasound is characterized by a broad (1-10 Hz) frequency content, whose peak changes from event to event (Figure 4a). In contrast, the seismic spectrum is characterized by a stable broad peak around 7 Hz for all events. The peak decreases rapidly below 2-3 Hz, well above the eigenfrequency of the Lennartz 3D seismometer, and above 20 Hz,

well below the Nyquist frequency (50 Hz) of the A/D converter.

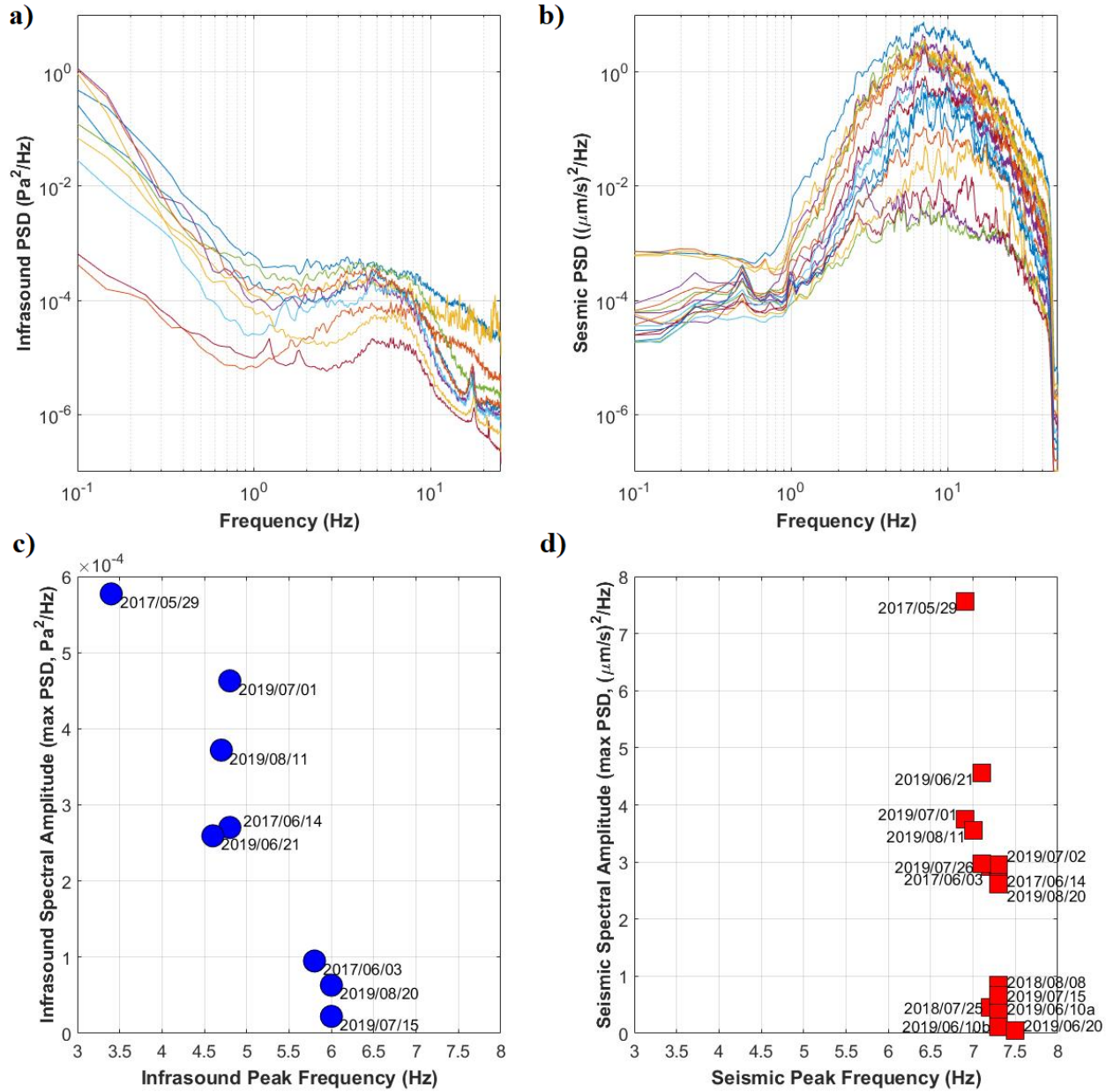


Figure 4: power spectral density of infrasound (a) and seismic (b) records of the Illgraben debris-flow events. Spectral peak amplitudes of infrasonic (c) and seismic (d) signals as a function of peak frequencies. In d) the two events on 2019/06/10 are marked in chronological order with the letters “a” and “b”.

Figure 4c and 4d show the comparison between maximum spectral amplitude (max PSD) and peak frequency values (f_P) of the signals. These were computed from PSDs as the weighted average of the frequency (f) over the spectral amplitude (Sa) (Table 2). For each event, the weighted average was calculated around ($df = 2$ Hz) of the manually picked peak frequency value (f_{mp}) as:

$$f_P = \frac{\sum_i Sa_i f_i}{\sum_i Sa_i} \quad f_i \in [f_{mp} - df, f_{mp} + df], \text{ (Eq. 4)}$$

Obtained infrasonic peak frequencies vary between 3.4 and 6 Hz (Table 2, Figure 4c), while seismic peak frequency is stable for all events, with values ranging between 6.8 and 7.2 Hz (Table 2, Figure 4d).

The frequency content of the infrasound generated by the events on 2019/07/02 and 2019/07/26 is strongly affected by the simultaneous thunderstorms (Figure 3a). Therefore, the infrasonic signals generated by these two events are excluded from Figure 4c and from the frequency analysis shown below in Figure 6.

In general, infrasound peak frequency tends to decrease with increasing spectral peak amplitude (Figure 4c). In contrast, such a relation between peak frequency and maximum spectral amplitude is much weaker or absent for seismic signals (Figure 4d).

1. Data Analysis and Results

5.1 Relationship between Seismo-Acoustic Amplitudes and Hydraulic Data

In order to investigate what fluid dynamic processes control the seismo-acoustic energy radiation by debris flows, the peak RMSA values (Table 2) of infrasound and seismic data are compared with available hydraulic data (Figure 5). The comparison is limited to events for which both seismo-acoustic and hydraulic data are available.

Results show a positive correlation between amplitude of seismo-acoustic signals (infrasonic and seismic max RMSA) and flow parameters. Concerning front velocity (Figure 5a and 5b), RMSA appears to increase with velocity, with the exemption of the slowest (1 m/s) and fastest (9 m/s) events, that prevents defining a clear correlation function.

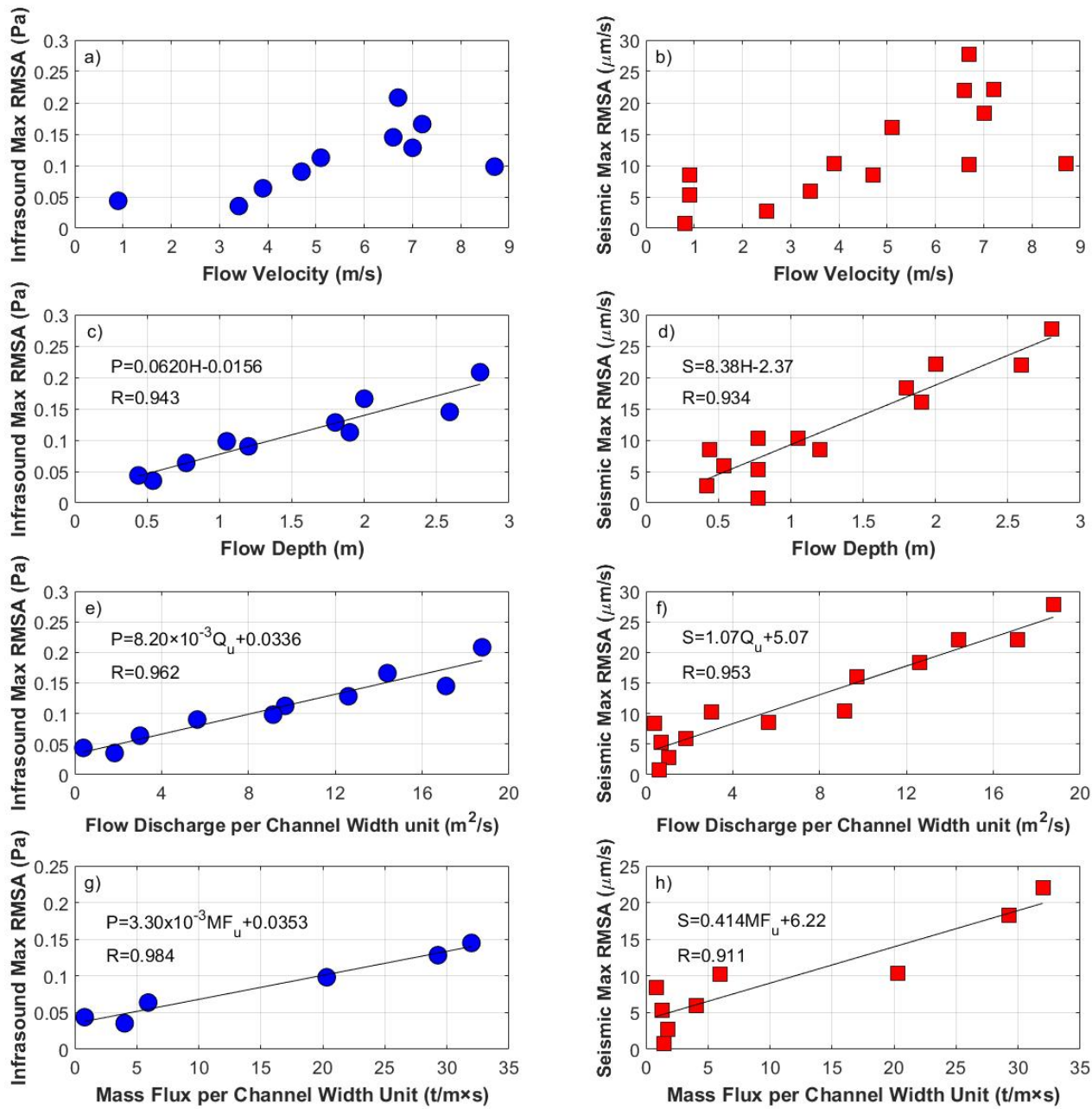


Figure 5: Relations between maximum RMSA of infrasonic (left side, blue circles) and seismic (right side, red squares) debris-flow signals and flow velocities (a, b), maximum flow depth (c, d), flow peak discharge per unit channel width

(e, f) and peak mass flux per unit channel width (g, h). In each diagram the best fit regression line is plotted and its equation is specified within the diagram. In the equations, P (in Pa) stands for infrasound max RMSA, S (in m/s) for seismic max RMSA, v is the front velocity (in m/s), H is the flow depth (in m), Q_u is the flow peak discharge per unit channel width (in m^2/s) and MF_u is the peak mass flux per unit channel width (in $t/m s$). For each best fit regression line, we computed the Pearson correlation factor R.

A clearer linear relationship, expressed with the Pearson correlation factor (R), is obtained considering the maximum flow depth (Figure 5c, d, $R=0.943$ and $R=0.950$ for infrasound and seismic signals respectively), and the peak discharge per unit channel width (Figure 5e, f, $R=0.962$ and $R=0.945$ for infrasound and for seismic signals, respectively). In particular the lowest amplitude signals are recorded for the smallest flows, with flow depth as low as 1 m and discharge as low as $3 m^2/s$, while signal amplitude increases with the flow depth and/or discharge.

Compared with seismo-acoustic maximum RMSA (Figure 5g, h), also the unit peak mass flux shows a linear relation ($R=0.984$ for infrasound, $R=0.906$ for seismic), suggesting that events with larger mass flux produce larger amplitude infrasound and seismic signals. However, in the comparison between seismo-acoustic amplitudes and unit mass flux, the combination of uncertainties linked to discharge and density estimations for the six selected events ($1930-2240 kg/m^3$, Table 1) and the lower number of available observations has to be considered when evaluating the quality of the obtained relation.

5.2 Relation between Seismo-Acoustic Peak Frequencies and Hydraulic Data

In order to investigate if the spectral content of infrasonic and seismic signals generated by debris-flows is controlled by a specific hydraulic parameter or physical process within the flow, available hydraulic data were compared to infrasonic and seismic signal peak frequencies (Figure 6), determined from computed PSD curves (Figure 4, Table 2). A systematic difference between peak frequencies of seismic and infrasound signals is observed (Figure 6): seismic peak frequency is stable around 7.1 Hz for all events (7.1 ± 0.2 Hz) regardless the size of the event, flow depth, velocity or discharge. On the contrary, infrasound peak frequency changes from event to event and decreases from 6 Hz to 3.4 Hz with increasing front velocity (Figure 6a), maximum flow depth (Figure 6b) or discharge per channel width (Figure 6c). Whereas the number of observations is still limited, this inverse relation between peak infrasound frequency and flow parameters seems however to be limited to larger events, exceeding velocities of 4 m/s, flow depth of 1-1.5 m, and peak discharge for unit width of $5 m^2/s$, while the relation is less evident for smaller and slower events.

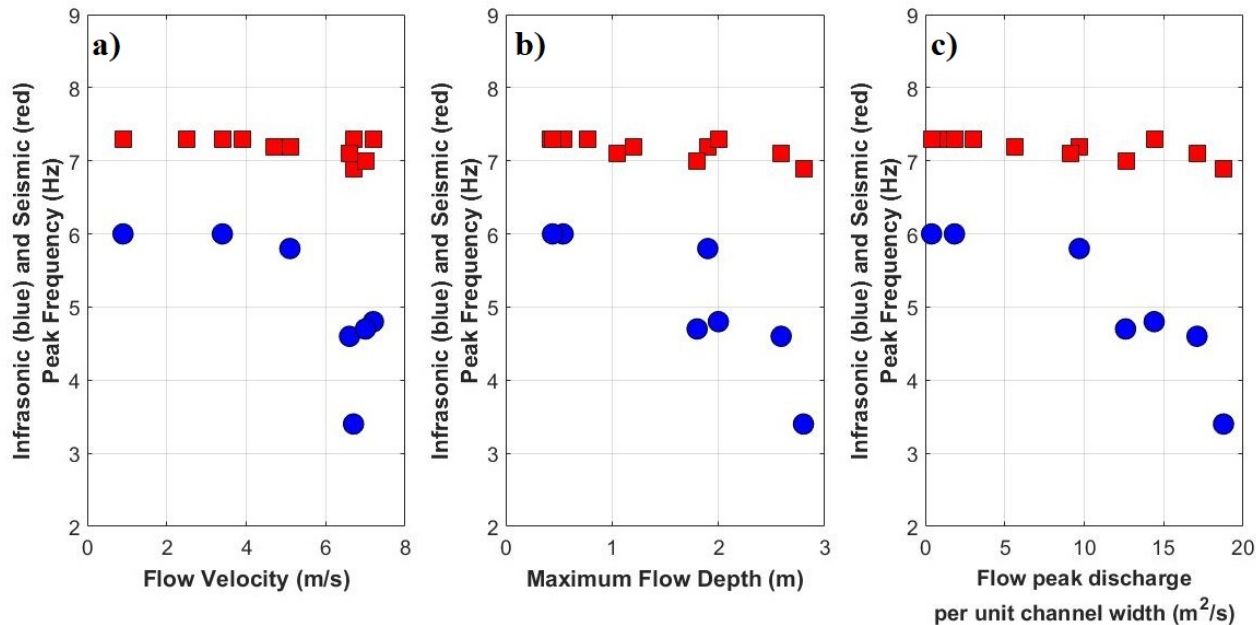


Figure 6: Relations between peak frequency of infrasonic (blue circles) and seismic (red squares) signals, generated by Illgraben debris-flows, and front velocity (a), maximum flow depth (b) and peak flow discharge per unit channel width (c). In each diagram, data points reflect debris-flow events for which the corresponding parameters (seismo-acoustic peak frequencies and front velocity, flow depth or discharge) are available or computable.

1. Discussion

The results presented in this study highlight general trends between infrasound and seismic observations of debris-flow activity at Illgraben and an evident positive correlation between maximum RMSA and flow parameters. Both seismic and infrasound energy radiation appears to be controlled by the flow characteristics, as shown by the linear relations between maximum RSMA and flow properties (Figure 5): higher flow velocities and/or larger flow depths generally produce higher amplitude infrasonic and seismic debris-flow signals. Despite some uncertainty for single data points, the measured high values of the Pearson correlation factor (R) shown in Figure 5c and d and in Figure 5e and f, suggest that flow depth and peak discharge per unit channel width control the amplitude of recorded seismo-acoustic signals.

Despite these similarities the infrasound and seismic signals show a decoupled frequency content. The seismic peak frequency is almost constant (6.9-7.3 Hz), regardless of the magnitude of the event (Figure 6). The measured value of ~ 7 Hz is in good agreement with the minimum distance of 550 m of the seismometer

to the Illgraben torrent, in accordance with the model proposed by Tsai et al. (2012) for seismic noise produced by bed load transport, that explains the frequency content in terms of propagation effects of surface waves and that was observed to be valid also for debris-flows (Lai et al., 2018; Wenner et al., 2019).

As opposed to the seismic data, infrasound peak frequency varies between 3.4 and 6 Hz and appears to systematically decrease with increasing event magnitude (flow depth and/or discharge) (Figure 6), suggesting that larger flows (events with larger discharge and/or flow depth) radiate lower frequency infrasound. This result is consistent with the findings by Marchetti et al., (2019), who analyzed only 3 debris-flow events that occurred in 2017 at the Illgraben (also included in this work), and by Coco et al. (2021), who modeled a decrease in peak frequency of infrasonic waves radiated by water flow downstream a topographic step (dam) with increasing flow depth or the height of the step. The inverse trend observed between infrasound peak frequency and flow magnitude holds for all considered hydraulic parameters (v , H and Q_u), but the best fit is obtained with the flow peak discharge per unit channel width (Figure 6c) rather than considering front velocity and maximum flow depth alone (Figure 6a, b). The best inverse relation is observed for larger events ($Q_u > 5 \text{ m}^2/\text{s}$). Infrasound peak frequency seems to be almost independent of flow discharge of smaller events. This could be at least partly explained by the signal-to-noise ratio, which affects determination of the peak frequency of smaller events.

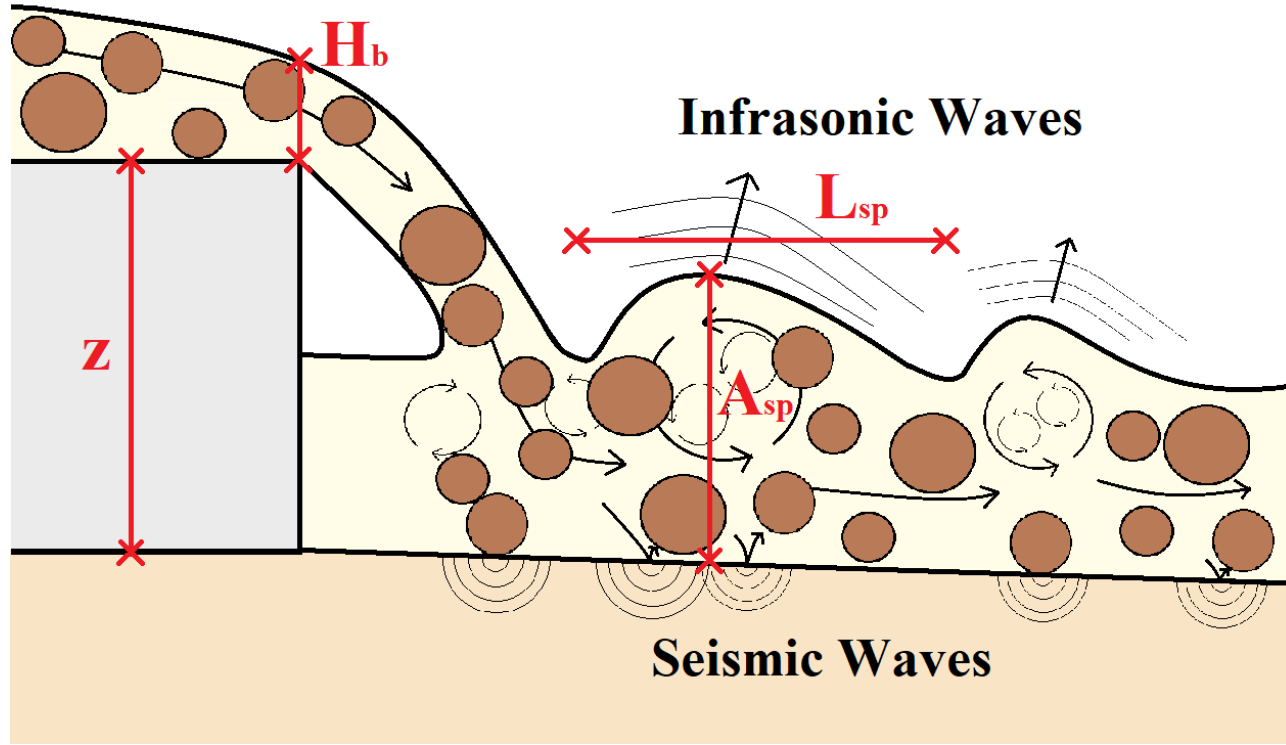


Figure 7: sketch of the source mechanism proposed for seismo-acoustic waves generated by debris-flows. z is the height of the topographic step; H_b is the flow depth over the brink of the free overfall; L_{sp} and A_{sp} are respectively the length and the amplitude (measured from the ground) of the waves or water splashes generated downstream the fall.

Such a variation of the infrasound frequency content suggests a complex relation to flow properties. According to fluid dynamic models and flume experiments on water flows, irregularities (waves and splashes) are induced at the flow surface by turbulence structures generated in the flow for water falling at free overfalls (Tokyay and Yildiz, 2007; Feng et al., 2014; Coco et al., 2021), such as dams, or for flow interaction with the channel roughness (Horoshenkov et al., 2013). In particular, Tokyay and Yildiz (2007) observed that at the base of a supercritical ($Fr > 1$) free overfall, there is strong energy dissipation (up to $>50\%$ of the initial energy) and the development of heavy water splashes at the flow's free surface (Figure 7), due to the flow impacting the floor and setting up vigorous circulation and turbulence. In particular, they observed that the height of the water splashes or waves linearly scales with the Froude number (Fr) (which increases with flow velocity) and with the square root of the product between the flow depth over the brink of the fall (H_b) and the height of the fall (z) as (Tokyay and Yildiz, 2007):

$$A_{\text{sp}} = 0.4532 Fr \sqrt{z H_b}, \text{ (Eq. 5)}$$

where the height of the water splash or waves A_{sp} is measured from the channel bottom (Figure 7). Such a flow behavior is to be expected also in case of debris-flows that undergo free-overfall at the check-dams, since computation of the Froude number (Figure 2e) revealed that larger ($H > 1$ m) Illgraben debris-flows all fall into the supercritical conditions. This scenario predicting increased turbulence downstream dams is in general agreement with Feng et al. (2014) who, based on the model by Ostrovsky and Bedard (2002) on infrasound produced by the fall of large objects into water, proposed that infrasonic waves are preferentially radiated at the base of dams by a dipole-type source generated by water falling into the absorption pole.

We did not account for elastic wave propagation. Relative signal comparison is still permissible, because the dominant signals are related to the passage of the “loudest” flow sections past the point along the torrent, which is closest to the recording station. For the seismic signals, our observed correlations thus agree with investigations using different Illgraben seismometers, which did quantify modifications of seismic frequency content and amplitudes as a result of propagation: high-frequency (> 1 Hz) seismic signals of Illgraben events were found to scale with the effective particle size in the coarse-grained flow front (Zhang et al., 2021(a)) and with flow depth (Zhang et al., 2021(b)). This agrees with theoretical predictions by Farin et al. (2019), although the exact scaling is difficult to capture, given that the flow parameters like flow depths, flow velocity, grain size distribution, particle sorting and water content all influence seismogenesis as well as each other.

Based on all presented results (Figure 5, 6), previous theoretical (Tsai et al., 2012; Gimbert et al., 2014; Farin et al., 2019) and numerical models (Coco et al., 2021) as well as field observations of infrasound and seismic signals radiated by debris flows (Schmandt et al., 2013; Kean et al., 2015; Lai et al., 2018; Marchetti et al., 2019; Belli et al., 2021), we propose a simplified conceptual source mechanism for seismo-acoustic waves radiated by debris-flows (Figure 7), with decoupled sources acting at the ground (seismic) and surface (infrasound) of the flow. Based on the signal-to-noise ratio, systematically higher for seismic signals compared to infrasound, we infer that debris-flows are likely more effective as seismic sources than as infrasound sources, especially for smaller magnitude events.

Concerning the seismic wave-field, because of the limited constraints we provide in this study, we rely on existing models for seismic energy radiation by rivers (Burtin et al., 2008; Tsai et al., 2012; Schmandt et al., 2013) and debris-flows (Burtin et al., 2009; Kean et al., 2015; Lai et al., 2018; Zhang et al., 2021(a)), which attribute the generation of seismic waves to solid particle collisions and friction with the channel bed and banks and fluid dynamic structures. In accordance with all these studies, our results confirm that the radiation of seismic-waves by debris-flows is strongly controlled by flow discharge (Figure 5).

An increased flow discharge leads to an increased transport capacity of the flow and to the development of larger fluid dynamic structures. An increased flow discharge leads to an increased transport capability of the solid fraction, with debris-flows able to transport boulders with a diameter as large as the flow depth (Badoux et al., 2009), a wider development of fluid dynamic structures (Tokyay and Yildiz, 2007) and a larger wetted perimeter. This scenario results in stronger and more frequent solid particle impacts and increased friction with channel bed and banks and thus leads to a higher amplitude seismic signal, while it doesn't affect the frequency content, that, being controlled solely by the source-to-receiver distance (Tsai et al., 2012), is expected to remain stable, in agreement with the experimental relations observed here (Figures 5, 6).

With the results of this study, particularly the inverse relation of infrasound frequency to flow properties, we can add constraints on a source mechanism of infrasound by the flow. In agreement with infrasound array analysis of debris-flows at the Illgraben (Marchetti et al., 2019, Belli et al. 2021), we suggest that infrasound by debris-flows is radiated along the entire length of the flow by turbulence induced free surface waves and oscillations, but is enhanced downstream of check dams. Indeed, such non-stationary water surface displacements are mostly generated where the turbulence is stronger and more powerful and therefore wherever the flow encounters significant channel irregularities (Henderson, 1996; Tokyay and Yildiz, 2007; Feng et al., 2014), such as topographic steps and steep bends in the planform geometry of the channel.

This interpretation is consistent with the experimental relations observed between infrasound maximum amplitude and debris-flow characteristics (Figure 5). An increase in the flow discharge enhances the development of a higher and more intense fluid dynamic turbulence in the flow, that induces larger waves and water splashes at the flow free surface (Tokyay and Yildiz, 2007), causing stronger pressure perturbations in the atmosphere and hence higher-amplitude infrasound waves (Ostrovsky and Bedard, 2002). Similarly, in agreement with flume experiments of supercritical water flows, the height (A_{sp}) and the wavelength (L_{sp}) of water splashes and non-stationary waves induced at the base of a free overfall (Figure 7) increase with increasing flow depth, flow velocity and the height of the fall (Tokyay and Yildiz, 2007), thus corroborating the observed experimental relation between infrasound amplitude and flow magnitude (Figure 5).

The proposed infrasound source mechanism based on turbulence induced non-stationary waves and splashes at the water free surface, developing mostly at topography changes (e.g. free-overfall at drop/dams) or channel irregularities (e.g. bends), is also in agreement with the observed decrease of the peak frequency with the increase of the discharge (Figure 6). Experimental (Tokyay and Yildiz, 2007) and numerical (Coco et al., 2021) results suggest that the wavelength of surface structures increases with the discharge, thus resulting in larger infrasonic sources and lower frequency infrasound. Numerical modeling (Coco et al., 2021) of infrasound waves produced by a river, indeed suggest a de-

crease of infrasound frequency when discharge increases for a fixed dam height, while it predicts the absence of significant infrasound radiation, regardless the flow discharge, when the flow occurs within flat channels lacking any irregularities (bed roughness topographic steps, bends). Furthermore, the infrasound source mechanism based on turbulence-induced surface oscillations discussed here also qualitatively explains the observed wide infrasound spectrum: turbulence structures, like eddies, cover a wide range of dimensions over which they also generate non-stationary flow surface displacements. This produces a wide frequency spectrum of pressure variation in the atmosphere (Feng et al., 2014).

Finally, the experimental relationships shown in this study suggest how geophysical data might be used for monitoring purposes at the Illgraben, and could provide, in real-time and without in-torrent measurement, an indirect estimate of flow depth and/or discharge from seismo-acoustic observations. Both the amplitude (Figure 5) and, for larger events, the frequency (Figure 6) of recorded infrasound could be used to estimate the discharge of the flow remotely. This further highlights the potential to use seismo-acoustic signals for debris-flow monitoring and risk management, not only for event detection (Walter et al., 2017; Marchetti et al., 2019; Chmiel et al., 2021), but also for real time estimates of debris-flow depth and or discharge.

Conclusions

We present a seismo-acoustic study of the debris-flow activity in the Illgraben catchment (Switzerland) during the period 2017-2019. In order to investigate what flow processes and parameter variations control the seismo-acoustic energy radiation by debris-flows, the amplitude and the spectral content of infrasonic and seismic signals are compared with flow measurements, i.e. flow front velocity, maximum flow depth and bulk flow density.

Results show that infrasonic and seismic maximum RMSA positively correlate with front velocity and scale linearly with maximum depth and flow peak discharge per unit channel width, computed as the product of front velocity and maximum depth. This indicates that flow velocity and flow depth combine to control the radiation of both seismic and infrasonic waves by debris-flows. A similar linear trend is observed also with the mass flux per unit channel width, obtained as the product of unit peak discharge and flow density. However, this comparison is limited to only six events for whom density was measured, preventing us from more accurately assessing the role of density and mass flux on seismo-acoustic radiation by debris-flows.

Spectral analysis of seismo-acoustic signals reveals that infrasonic and seismic signals of debris-flows are characterized by different peak frequencies. We show that unlike seismic signals that, in agreement with previous studies, are characterized by a nearly constant peak frequency regardless of the flow size, infrasound peak frequency decreases with increasing front velocity, flow depth and discharge.

Based on presented results and taking into account previous models and exper-

iments, we propose a decoupled source mechanism for seismic and infrasound radiation by the flow. Results agree with previous models and observation of seismic energy radiation by rivers (Burtin et al., 2008; Tsai et al., 2012; Schmandt et al., 2013) and debris-flows (Burtin et al., 2009; Kean et al., 2015; Lai et al., 2018; Zhang et al., 2021(a)), indicating that seismic waves are generated by solid particle collisions and friction with the river bed and banks and by fluid dynamic structures.

For infrasound we propose a source mechanism in which infrasonic waves are generated by turbulence-induced waves and oscillations that develop at the free surface of the flow (Ostrovsky and Bedard, 2002; Feng et al., 2014; Marchetti et al., 2019). The formation of such surface waves is enhanced wherever the flow encounters channel irregularities, such as significant topographic steps and steep bends (Tokyay and Yildiz, 2007; Belli et al., 2021; Coco et al., 2021). Here, an increase in the flow discharge enhances the development of larger turbulent flow structures, that generate larger waves and turbulence-induced water splashes at the flow free surface (Tokyay and Yildiz, 2007), thus radiating higher-amplitude infrasound waves (Marchetti et al., 2019; Coco et al., 2021). Numerical (Coco et al., 2021) and experimental (Tokyay and Yildiz, 2007) studies suggest that the flow discharge and the dimensions of irregularities affect the wavelength of turbulence-induced surface structures thus controlling the frequencies of recorded infrasound.

Presented results, linking seismo-acoustic signal features to flow properties, allow to investigate the source processes of the two wave fields within debris-flows and thus provide a valuable observational basis for future theoretical and experimental studies. Moreover, the observed relationships between seismo-acoustic signal features and flow parameters suggests how infrasound and seismic signals could be used for the near real-time estimation of the size of an ongoing debris-flow, highlighting their potential for debris-flow monitoring and risk management.

Acknowledge

Infrasound data, recorded by ILG arrays, used to achieve all the findings and create all the figures in this paper, are freely available in the Open Science framework repository (<https://osf.io/36nvq/>).

Seismic data from the Illgraben network are collected under the network code XP (<https://doi.org/10.12686/sed/networks/xp>) and all seismic data will be openly available after a 2-year embargo (in 2023) via the archives in the Swiss Seismological Service, <http://www.seismo.ethz.ch/en/research-and-teaching/products-software/waveform-data/>, and in the European Integrated Data Archive (EIDA), <http://www.orfeus-eu.org/data/eida/>.

References

Allstadt, K. E., Matoza, R. S., Lockhart, A. B., Moran, S. C., Caplan-Auerbach, J., Haney, M. M., ... & Malone, S. D. (2018). Seismic and acoustic signatures of

- surficial mass movements at volcanoes. *Journal of Volcanology and Geothermal Research*, 364, 76-106.
- Arattano, M. (1999). On the use of seismic detectors as monitoring and warning systems for debris flows. *Natural Hazards*, 20(2-3), 197-213.
- Badoux, A., Graf, C., Rhyner, J., Kuntner, R., & McArdell, B. W. (2009). A debris-flow alarm system for the Alpine Illgraben catchment: design and performance. *Natural hazards*, 49(3), 517-539.
- Belli, G., Marchetti, E., Walter, F., McArdell, B., Chmiel, M., and Wenner, M.: Investigating infrasound sources within Illgraben debris-flows, EGU General Assembly 2021, online, 19–30 Apr 2021, EGU21-1226, <https://doi.org/10.5194/egusphere-egu21-1226>, 2021.
- Bennett, G. L., Molnar, P., McArdell, B. W., Schlunegger, F., & Burlando, P. (2013). Patterns and controls of sediment production, transfer and yield in the Illgraben. *Geomorphology*, 188, 68-82.
- Berger, C., McArdell, B. W., & Schlunegger, F. (2011). Direct measurement of channel erosion by debris flows, Illgraben, Switzerland. *Journal of Geophysical Research: Earth Surface*, 116(F1).
- Bowman, J. R., Baker, G. E., and Bahavar, M. (2005), Ambient infrasound noise, *Geophys. Res. Lett.*, 32, L09803, doi:10.1029/2005GL022486.
- Burtin, A., Bollinger, L., Cattin, R., Vergne, J., & Nábělek, J. L. (2009). Spatiotemporal sequence of Himalayan debris flow from analysis of high-frequency seismic noise. *Journal of Geophysical Research: Earth Surface*, 114(F4).
- Burtin, A., Bollinger, L., Vergne, J., Cattin, R., & Nábělek, J. L. (2008). Spectral analysis of seismic noise induced by rivers: A new tool to monitor spatiotemporal changes in stream hydrodynamics. *Journal of Geophysical Research: Solid Earth*, 113(B5).
- Burtin, A., Hovius, N., McArdell, B. W., Turowski, J. M., & Vergne, J. (2014). Seismic constraints on dynamic links between geomorphic processes and routing of sediment in a steep mountain catchment. *Earth Surface Dynamics*, 2(1), 21.
- Chmiel, M., Walter, F., Wenner, M., Zhang, Z., McArdell, B. W., & Hibert, C. (2021). Machine Learning improves debris flow warning. *Geophysical Research Letters*, 48(3), e2020GL090874.
- Chou, H. T., Chang, Y. L., & Zhang, S. C. (2013). Acoustic signals and geophone response of rainfall-induced debris flows. *Journal of the Chinese Institute of Engineers*, 36(3), 335-347.
- Coco, M., Marchetti, E., & Morandi, O. (2021). Numerical Modeling of Infrasound Energy Radiation by Debris Flow Events. *Pure and Applied Geophysics*, 1-13.

- Costa, J. E., & Williams, G. P. (1984). Debris-flow dynamics: US Geological Survey Open File Report 84-606, 1 VHS videotape.
- Coussot, P., & Meunier, M. (1995). Experimental Study of Debris Flows. *Journal of Hydraulic Engineering*, 121(5), 438-440.
- Coussot, P., & Meunier, M. (1996). Recognition, classification and mechanical description of debris flows. *Earth-Science Reviews*, 40(3-4), 209-227.
- Coussot, P., & Piau, J. M. (1994). Rheology of very concentrated suspensions of force-free particles. *Les Cahiers de Rhéologie*, 13, 266-277.
- Coviello, V., Arattano, M., Comiti, F., Macconi, P., & Marchi, L. (2019). Seismic characterization of debris flows: insights into energy radiation and implications for warning. *Journal of Geophysical Research: Earth Surface*, 124(6), 1440-1463.
- Dowling, C. A., & Santi, P. M. (2014). Debris flows and their toll on human life: a global analysis of debris-flow fatalities from 1950 to 2011. *Natural hazards*, 71(1), 203-227.
- Estep, J., & Dufek, J. (2012). Substrate effects from force chain dynamics in dense granular flows. *Journal of Geophysical Research: Earth Surface*, 117(F1).
- Farin, M., Tsai, V. C., Lamb, M. P., & Allstadt, K. E. (2019). A physical model of the high-frequency seismic signal generated by debris flows. *Earth Surface Processes and Landforms*, 44(13), 2529-2543.
- Feng, H. N., Yang, Y. C., Chunchuzov, I. P., & Teng, P. X. (2014). Study on Infrasound From a Water Dam. *Acta Acustica united with Acustica*, 100(2), 226-234.
- Gimbert, F., Tsai, V. C., & Lamb, M. P. (2014). A physical model for seismic noise generation by turbulent flow in rivers. *Journal of Geophysical Research: Earth Surface*, 119(10), 2209-2238.
- Gregoretto, C., & Dalla Fontana, G. (2008). The triggering of debris flow due to channel-bed failure in some alpine headwater basins of the Dolomites: Analyses of critical runoff. *Hydrological Processes: An International Journal*, 22(13), 2248-2263.
- Henderson, F. M. (1996). Open channel flow.
- Horoshenkov, K. V., Nichols, A., Tait, S. J., & Maximov, G. A. (2013). The pattern of surface waves in a shallow free surface flow. *Journal of Geophysical Research: Earth Surface*, 118(3), 1864-1876.
- Hürlimann, M., Rickenmann, D., & Graf, C. (2003). Field and monitoring data of debris-flow events in the Swiss Alps. *Canadian geotechnical journal*, 40(1), 161-175.
- Hürlimann, M., Coviello, V., Bel, C., Guo, X., Berti, M., Graf, C., ... & Yin, H. Y. (2019). Debris-flow monitoring and warning: Review and examples. *Earth-science reviews*, 199, 102981.

- Iverson, R. M. (1997, August). Hydraulic modeling of unsteady debris-flow surges with solid-fluid interactions. In *Proceedings, First International Conference on Debris-Flow Hazards Mitigation: Mechanics, Prediction, and Assessment: Hydraulics Division, American Society of Civil Engineers* (pp. 550-560).
- Iverson, R. M., & Vallance, J. W. (2001). New views of granular mass flows. *Geology*, *29*(2), 115-118.
- Iverson, R. M., Reid, M. E., & LaHusen, R. G. (1997). Debris-flow mobilization from landslides. *Annual Review of Earth and Planetary Sciences*, *25*(1), 85-138.
- Ivy-Ochs, S., Kerschner, H., Reuther, A., Preusser, F., Heine, K., Maisch, M., ... & Schlüchter, C. (2008). Chronology of the last glacial cycle in the European Alps. *Journal of Quaternary Science: Published for the Quaternary Research Association*, *23*(6-7), 559-573.
- Johnson, A. M. (1970). Physical processes in geology: A method for interpretation of natural phenomena; intrusions in igneous rocks, fractures, and folds, flow of debris and ice. Freeman, Cooper.
- Johnson, A. M., & Rodine, J. R. (1984). Debris flow (Chapter 8). Slope Instability, eds. D. Brunsten & DB Prior.
- Kean, J. W., Coe, J. A., Coviello, V., Smith, J. B., McCoy, S. W., & Arattano, M. (2015). Estimating rates of debris flow entrainment from ground vibrations. *Geophysical Research Letters*, *42*(15), 6365-6372.
- Khegai, A. Y., Popov, N. V., Plekhanov, P. A., & Keremkulov, V. A. (1992). Experiments at the Chemolgan debris-flow testing ground, Kazakhstan, *Landslide News*, *6*, 27-28, Jpn. Landslide Soc., Kyoto.
- Kudo, N. (1993). Control of infrasonic noise from a waterfall. *Journal of Low Frequency Noise, Vibration and Active Control*, *12*(4), 149-155.
- Lai, V. H., Tsai, V. C., Lamb, M. P., Ulizio, T. P., & Beer, A. R. (2018). The seismic signature of debris flows: Flow mechanics and early warning at Montecito, California. *Geophysical Research Letters*, *45*(11), 5528-5535.
- Marchetti, E., Walter, F., Barfucci, G., Genco, R., Wenner, M., Ripepe, M., ... & Price, C. (2019). Infrasonic array analysis of debris flow activity and implication for early warning. *Journal of Geophysical Research: Earth Surface*, *124*(2), 567-587.
- McArdell, B. W. (2016). Field measurements of forces in debris flows at the Illgraben: implications for channel-bed erosion. *International Journal of Erosion Control Engineering*, *9*(4), 194-198.
- McArdell, B. W., Bartelt, P., & Kowalski, J. (2007). Field observations of basal forces and fluid pore pressure in a debris flow. *Geophysical research letters*, *34*(7).

- Ostrovsky, L. A. (2002, June). On generation of infrasound by large objects falling into water. In *IEEE International Geoscience and Remote Sensing Symposium* (Vol. 2, pp. 873-875). IEEE.
- Pérez, F. L. (2001). Matrix granulometry of catastrophic debris flows (December 1999) in central coastal Venezuela. *Catena*, *45*(3), 163-183.
- Pierson, T. C. (1980). Erosion and deposition by debris flows at Mt Thomas, north Canterbury, New Zealand. *Earth Surface Processes*, *5*(3), 227-247.
- Pierson, T. C. (1985). Effects of slurry composition on debris flow dynamics, Rudd Canyon, Utah. Delineation of Landslide, Flash Flood, and Debris-Flow Hazard in Utah, Logan, Utah Water Research Laboratory, Utah State University, General series UWRL/G.
- Pierson, T. C. (1986). Flow behavior of channelized debris flows Mount St. Helens Washington. *Hillslope processes*, 269-296.
- Pierson, T. C., Costa, J. E., & Vancouver, W. (1987). A rheologic classification of subaerial sediment-water flows. Debris flows/avalanches: process, recognition, and mitigation. *Reviews in Engineering Geology*, *7*, 1-12.
- Rickenmann, D., Hürlimann, M., Graf, C., Näf, D., & Weber, D. (2001). Murgang-beobachtungsstationen in der Schweiz. *Wasser Energie Luft*, *93*(1/2), 1-8.
- Ripepe, M., De Angelis, S., Lacanna, G., Poggi, P., Williams, C., Marchetti, E., ... & Olivieri, G. (2009). Tracking pyroclastic flows at Soufrière Hills volcano. *Eos, Transactions American Geophysical Union*, *90*(27), 229-230.
- Schimmel, A., Coviello, V., & Comiti, F. (2021). Debris-flow velocity and volume estimations based on seismic data. *Natural Hazards and Earth System Sciences Discussions*, 1-21.
- Schimmel, A., Hübl, J., McArdeell, B. W., & Walter, F. (2018). Automatic identification of alpine mass movements by a combination of seismic and infrasound sensors. *Sensors*, *18*(5), 1658.
- Schlunegger, F., Badoux, A., McArdeell, B. W., Gwerder, C., Schnydrig, D., Rieke-Zapp, D., & Molnar, P. (2009). Limits of sediment transfer in an alpine debris-flow catchment, Illgraben, Switzerland. *Quaternary Science Reviews*, *28*(11-12), 1097-1105.
- Schmandt, B., Aster, R. C., Scherler, D., Tsai, V. C., & Karlstrom, K. (2013). Multiple fluvial processes detected by riverside seismic and infrasound monitoring of a controlled flood in the Grand Canyon. *Geophysical Research Letters*, *40*(18), 4858-4863.
- Schürch, P., Densmore, A. L., Ivy-Ochs, S., Rosser, N. J., Kober, F., Schlunegger, F., ... & Alifimov, V. (2016). Quantitative reconstruction of late Holocene surface evolution on an alpine debris-flow fan. *Geomorphology*, *275*, 46-57.

- Sharp, R. P., & Nobles, L. H. (1953). Mudflow of 1941 at Wrightwood, southern California. *Geological Society of America Bulletin*, 64(5), 547-560.
- Smart, G., & Jäggi, M. (1983). Sediment transport on steep slopes. Mitteilung. 64. *Versuchsanstalt für Wasserbau, Hydrologie und Glaziologie*.
- Takahashi, T. (1981). Debris flow. *Annual review of fluid mechanics*, 13(1), 57-77.
- Tokyay, N. D., & Yildiz, D. (2007). Characteristics of free overfall for supercritical flows. *Canadian Journal of Civil Engineering*, 34(2), 162-169.
- Tsai, V. C., Minchew, B., Lamb, M. P., & Ampuero, J. P. (2012). A physical model for seismic noise generation from sediment transport in rivers. *Geophysical Research Letters*, 39(2).
- Ulivieri, G., Marchetti, E., Ripepe, M., Chiambretti, I., De Rosa, G., & Segor, V. (2011). Monitoring snow avalanches in Northwestern Italian Alps using an infrasound array. *Cold Regions Science and Technology*, 69(2-3), 177-183.
- Vilajosana, I., Surinach, E., Abellán, A., Khazaradze, G., Garcia, D., & Llosa, J. (2008). Rockfall induced seismic signals: case study in Montserrat, Catalonia. *Nat. Hazards Earth Syst. Sci*, 8(4), 805-812.
- Walter, F., Burtin, A., McArdell, B. W., Hovius, N., Weder, B., & Turowski, J. M. (2017). Testing seismic amplitude source location for fast debris-flow detection at Illgraben, Switzerland. *Natural Hazards and Earth System Sciences*, 17(6), 939-955.
- Wang, B., Li, Y., Liu, D., & Liu, J. (2018). Debris flow density determined by grain composition. *Landslides*, 15(6), 1205-1213.
- Wenner, M., Walter, F., McArdell, B., & Farinotti, D. (2019). Deciphering debris-flow seismograms at Illgraben, Switzerland. In *Association of Environmental and Engineering Geologists; special publication 28*. Colorado School of Mines. Arthur Lakes Library.
- Yamasato, H. (1997). Quantitative analysis of pyroclastic flows using infrasonic and seismic data at Unzen volcano, Japan. *Journal of Physics of the Earth*, 45(6), 397-416.
- Zhang, Z., Walter, F., McArdell, B. W., de Haas, T., Wenner, M., Chmiel, M., & He, S. (2021) (b). Analyzing bulk flow characteristics of debris flows using their high frequency seismic signature. *Journal of Geophysical Research: Solid Earth*, e2021JB022755.
- Zhang, Z., Walter, F., McArdell, B. W., Wenner, M., Chmiel, M., de Haas, T., & He, S. (2021) (a). Insights from the particle impact model into the high frequency seismic signature of debris flows. *Geophysical Research Letters*, e2020GL088994.